Applied Physics Letters

RESEARCH ARTICLE | SEPTEMBER 03 2024

Origin of zero thermal expansion in an average cubic structure in Pb-free relaxor ferroelectrics

Anuvrat Tripathi ; Abhishek Pandey ; Jose Antonio Alonso ; Rudolph Erasmus ; Maria Teresa Fernandez-Diaz ; Saurabh Tripathi

Appl. Phys. Lett. 125, 102901 (2024)
https://doi.org/10.1063/5.0219631

AIP Publishing

Applied Physics Letters ARTICLE pubs.aip.org/aip/apl

Origin of zero thermal expansion in an average cubic structure in Pb-free relaxor ferroelectrics

Cite as: Appl. Phys. Lett. **125**, 102901 (2024); doi: 10.1063/5.0219631
Submitted: 18 May 2024 · Accepted: 14 August 2024 ·
Published Online: 3 September 2024

Anuvrat Tripathi,[1] Abhishek Pandey,[2] Jose Antonio Alonso,[3] Rudolph Erasmus,[4] Maria Teresa Fernandez-Diaz,[5] and Saurabh Tripathi[1,a)]

AFFILIATIONS

[1]Department of Physics, Indian Institute of Technology (BHU), Varanasi 221005, India
[2]Materials Physics Research Institute, School of Physics, University of the Witwatersrand, Johannesburg, 2000 Gauteng, South Africa
[3]Instituto de Ciencia de Materiales de Madrid, C.S.I.C., Cantoblanco, E-28049 Madrid, Spain
[4]Materials for Energy Research Group, Material Physics Research Institute, School of Physics, University of the Witwatersrand, Johannesburg 2000, South Africa
[5]Institut Laue Langevin BP156 X, 38042 Grenoble Cedex, France

[a)]Author to whom correspondence should be addressed: stripathi.phy@itbhu.ac.in

ABSTRACT

This study presents "$K_{0.5}Na_{0.5}NbO_3$-based" Pb-free smart material $0.80(K_{0.5}Na_{0.5}NbO_3)$–$0.20(Ba_{0.9}Sr_{0.1}TiO_3)$ (KBST20) as exhibiting zero thermal expansion (ZTE) at low temperatures ($T \leq 100$ K) with long-range cubic symmetry stable over a wide temperature range (9 K $\leq T \leq$ 500 K). The linear coefficient of the thermal expansion (α_l) obtained from temperature-dependent neutron diffraction data is in the range of $0.255–5.75 \times 10^{-6}$ K^{-1} (9–500 K), which is rarely observed for Pb-free materials possessing long-range cubic symmetry. The temperature-dependent dielectric data of KBST20 exhibits a strong relaxational behavior with high frequency dispersion ($\Delta T \approx 27$ K), suggesting the presence of polar phased regions known as polar nano regions. The ZTE has been attributed to enhanced correlations among PNRs exhibiting ferroelectrostriction. Furthermore, temperature-dependent Raman scattering data reveal polar monoclinic distortion at short ranges rather than cubic symmetry at long ranges. In addition, the intensity of Raman modes increases with the decrease in temperature, suggesting enhancement of the polar phase at low temperatures, which consequently leads to zero thermal expansion in KBST20.

Controlled thermal expansion driven thermal stability is a vital requirement for modern electronic devices, viz., solid oxide fuel cells, micropositioners, actuators, multi-layer ceramic capacitors, thin films, and many others.[1–6] Thermal stability can be achieved using materials possessing negative thermal expansion (NTE)/ZTE. These materials include various types of structures, such as open framework structures in ZrW_2O_8 (Ref. 7) and ScF_3,[8] magnetic structures in Fe–Ni invar alloys[9] and Mn_3Ge,[10] superconductors, viz., MgB_2 (Ref. 11) and $NdFeAsO_{0.89}F_{0.11}$,[12] ferroelectric structures, viz., $PbTiO_3$ (Refs. 13 and 14) and $Pb(Ti,V)O_3$,[15] and non-polar disordered perovskites/relaxor ferroelectrics (RFEs), viz., $Pb(Zn, Nb)O_3$,[16] $Pb(Fe,Nb)O_3$,[17] $Ba(Zr,Ti)O_3$,[18] and $Pb(Mg,Nb)O_3$.[19,20] Among these, NTE in perovskite (ABO_3) based ferroelectrics results from the strong covalent character of A/B–O bonds, consequently leading to ferroelectrostriction.[21] For instance, materials such as $PbTiO_3$, $PbVO_3$, and $Pb(Ti,V)O_3$ with tetragonal structure at long-ranges exhibit high ferroelectrostriction due to the strong covalent nature of Pb–O and Ti/V–O bonds, thereby resulting in NTE.[15,21–23] Moreover, ferroelectrostriction observed in $BaTiO_3$ and $KNbO_3$ arises from the covalent character of Ti–O and Nb–O bonds, respectively.[22,24,25] NTE can also be observed in technologically important non-polar disordered perovskites/RFEs due to cationic ordering, which can be achieved by temperature, pressure, frequency, and electric field.[26,27]

The synergistic coupling of RFEs with ZTE may lead to technologically important smart materials useful for various applications, viz., sensors and actuators, micropositioners, medical imaging devices, and many others.[30,31] The relaxor materials exhibit broad and diffuse dielectric peaks for various frequencies.[32,33] The diffuseness of dielectric peak in RFEs is due to the heterovalent substitution/ionic radii mismatch of cations, whereas the distribution of various polar nano regions (PNRs) is responsible for frequency dispersion.[34,35] The existence of PNRs has a significant influence on the lattice dynamics of relaxor ferroelectrics and can be attributed to the thermal behavior of materials.[36,37]

The relaxor properties are common to various oxide-based perovskites, viz., $Pb(Mg_{1/3}Nb_{2/3})O_3$, $Pb(Mg_{1/3}Nb_{2/3})O_3$-$x$$PbTiO_3$,[38] Ba(Zr, Ti)$O_3$-based ceramics,[39] and $K_{0.5}Na_{0.5}NbO_3$ (KNN50)-based ceramics such as KNN50-$x$$BaTiO_3$ (KNN50-xBT),[40] KNN50-x(Ba,Sr)TiO_3 (KNN50-xBST),[41,42] etc.[43,44] Among various RFE, Pb-based materials are widely studied for ZTE behavior.[20] Owing to detrimental effects of Pb, various Pb-free alternatives, viz., $Li_{0.2}Na_{0.8}NbO_3$[45] and KNN50,[46] are being studied for their scientific and technological aspects.[45,46] Among these, KNN50 is known to exhibit physical properties comparable to Pb-based materials.[46,47] However, it does not exhibit relaxor properties. In a recent letter on $BaTiO_3$ doped KNN50, viz., KNN50-$x$$BaTiO_3$ (KBTx), Yang *et al.* have reported unique physical properties of the compositions exhibiting relaxor/diffuse properties.[40] Among various compositions, the dielectric response is maximum at ambient conditions for $x = 0.20$.[40] Furthermore, several authors doped strontium (Sr) at A-site in KBTx to develop high-temperature Pb-free relaxor ferroelectrics useful for various applications, viz., aerospace, automotive, and many others.[41,42]

In the present work, we have selected $Ba_{0.9}Sr_{0.1}TiO_3$ (BST10) due to the maximum dielectric response[48–51] and synthesized the solid solution of KNN50 with BST10, viz., 0.80(KNN50)-0.20(BST10) (KBST20). The long- and short-range symmetries of KBST20 were determined using temperature-dependent neutron diffraction and Raman spectroscopy data, respectively. Temperature-dependent dielectric data and hysteresis loops were used to analyze the relaxor properties and expected ordering at low temperatures. The lattice parameters and volume were determined by Le Bail analysis. Furthermore, the linear coefficient of thermal expansion [CTE (α_l)] and spontaneous volume ferroelectrostriction (SVFS) were calculated.

The KBST20 composition was synthesized using a solid-state reaction method (see the supplementary material for details). Temperature-dependent neutron diffraction data ($9\,K \leq T \leq 500\,K$) were obtained from the D1B diffractometer at the Institut Laue-Langevin, Grenoble. The observed diffraction pattern shows the formation of a solid solution [Fig. 1(a)]. All reflections in the diffraction patterns exhibit a singlet nature, suggesting the cubic structure [Figs. 1(b)–1(d)]. Owing to the singlet nature of the peaks, the diffraction patterns were refined with the $Pm\bar{3}m$ space group via the Le Bail method (see the supplementary material) available in the FULLPROF[52] package. Figure 1(e) depicts the evolution of volume as a function of temperature. The volume shows nearly linear behavior above the Burns temperature (T_B; determined from dielectric data), while it shows a nonlinear behavior below T_B with a tendency to saturation at low temperatures below ≈ 100 K. Moreover, at low temperatures ($T \lesssim 100$ K), the volume becomes nearly temperature-independent [Fig. 1(e)], suggesting ZTE in the material. In order to quantify ZTE, we have calculated the volumetric coefficient of thermal expansion (α_V) using the following equation:[21]

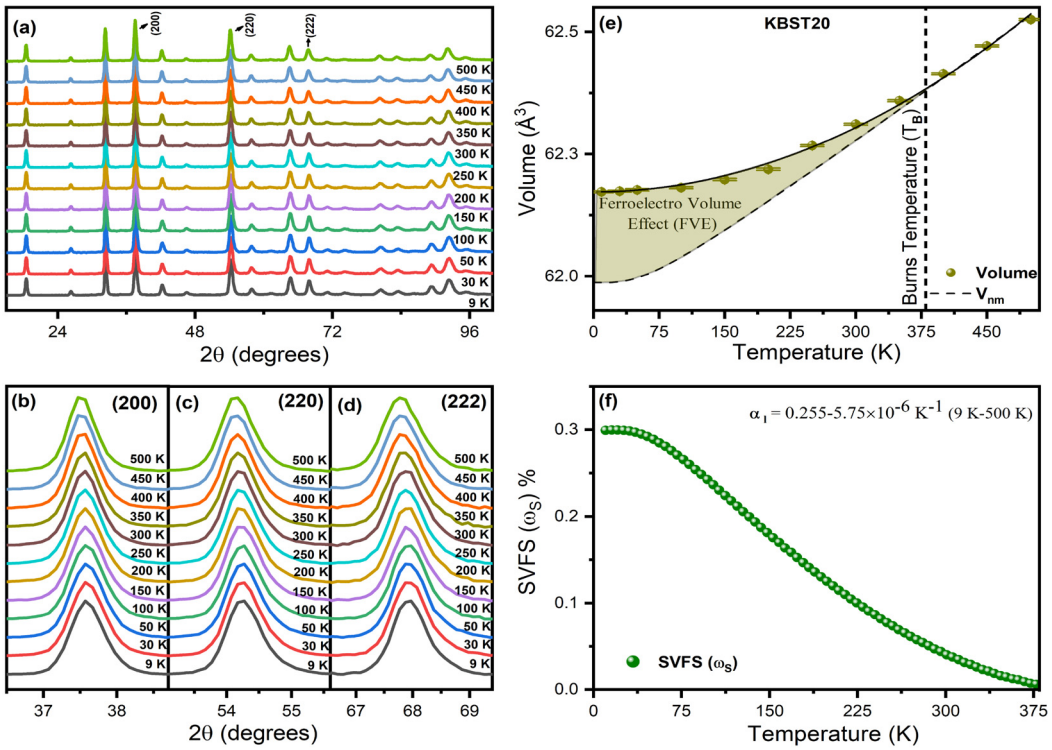

FIG. 1. (a) Temperature-dependent neutron diffraction data of pure KBST20 ceramic, (b)–(d) temperature-dependent evolution of (200), (220), and (222) peaks, respectively, (e) temperature-dependent variation of volume for KBST20 ceramic, where the symbol represents the experimental volume, the solid curve represents the polynomial fit of the experimental volume, and the dashed curve represents the nominal volume obtained from the fitting of the Debye–Gr $\ddot{u}$ neisen equation for $380\,K \leq T \leq 500\,K$.[21,28,29] (f) Variation of SVFS (ω_s) with temperature for $9\,K \leq T \leq 380\,K$, where SVFS has been calculated using the interpolated volume data.

$$\alpha_V = \frac{1}{V}\frac{\partial V}{\partial T}, \tag{1}$$

where V is the volume at temperature T.[21,28] For cubic systems, the linear α_l equals one-third of the volumetric α_V, i.e., $\alpha_l = \frac{1}{3}\alpha_V$.[21] Here, for KBST20 ceramics, α_l and α_V ranges from $0.255–5.75 \times 10^{-6}$ K^{-1} (9–500 K) and $0.765–17.25 \times 10^{-6}$ K^{-1} (9–500 K), respectively thereby confirming ZTE in the material. The obtained CTE values are compared to CTE values of various other oxide perovskites (see Table S1).

NTE/ZTE in ferroelectric materials is observed due to high ferroelectricity resulting from the strong covalent character of *A*–O and (or) *B*–O bonds, referred to as ferroelectrostriction.[21] Ferroelectrostriction leads to volume gain at low temperatures, often referred to as the ferroelectrovolume effect (FVE).[20,21] Here, for KBST20 ceramics, the observed volume gain at low temperatures [Fig. 1(e)] is quantitatively described by using a recently evolved quantifier known as spontaneous volume ferroelectrostriction (SVFS) ω_S,[15,21,53]

$$\omega_s = \frac{V_{exp} - V_{nm}}{V_{nm}} \times 100\%, \tag{2}$$

where V_{exp} and V_{nm} correspond to experimental and nominal volumes, respectively. V_{nm} is the extrapolated value of volume obtained after fitting the Debye–Grüneisen equation (see the supplementary material). V_{nm} represents the contribution from lattice (phonon) vibrations.[15,21,53] Large values of SVFS result from high ferroelectrostriction, which leads to NTE/ZTE in the material.[21,53] Figure 1(f) depicts SVFS as a function of temperature for KBST20. It is clearly evident from the figure that the SVFS increases ($\omega_S \approx 0.3\%$ at 9 K) with the decrease in temperature, thereby suggesting ZTE.

Figure 2(a) depicts the variation of dielectric permittivity (ε') and loss ($\tan\delta$) as a function of temperature ($105\,K \leq T \leq 650\,K$). The ε' and $\tan\delta$ exhibit observable contributions from electrical conductivity or space charge at low frequencies for high temperatures [Fig. 2(a)].[41]

We observe a broad and diffuse dielectric peak with strong frequency dispersion ($\Delta T \approx 27$ K) and dielectric maxima ($\varepsilon_{max} \approx 1708$ at 10 kHz) near the room temperature ($T_m \approx 315$ K) [Fig. 2(b)]. The diffuse broad peak, frequency dispersion, and an invariant long-range symmetry throughout are the relaxors' signature.[32–34,43] Moreover, the dielectric permittivity curve deviates from the Curie–Weiss law for materials exhibiting diffuse phase transitions (DPT) and (or) relaxor behavior.[34,41,43] This deviation starts from Burn's temperature (T_B) and is determined from the inverse dielectric permittivity plotted as a function of temperature (i.e. $1/\varepsilon'$ vs T) [Fig. 2(c)].

Owing to the relaxor properties of KBST20, the dielectric function can be fitted by the modified Curie–Weiss law formulated by Uchino and Nomura as[41,54]

$$\frac{1}{\varepsilon'} - \frac{1}{\varepsilon'_{max}} = \frac{(T - T_m)^\gamma}{C}, \tag{3}$$

where C is the Curie constant, and γ is the diffusion exponent lying between $1 \leq \gamma \leq 2$. Here, $\gamma = 1$ corresponds to normal ferroelectrics, and $\gamma = 2$ corresponds to an ideal relaxor.[41,54] The value of γ obtained after fitting the modified Curie–Weiss law is 1.87 [Fig. 2(d)], which also suggests the relaxor behavior of the material. The relaxor properties in KBST20 are induced due to the presence of the heterovalent character of ions and ionic radii mismatch of *A*-site ($r^{2+}_{Ba} = 161$ pm, $r^{2+}_{Sr} = 144$ pm, $r^{1+}_{K} = 164$ pm, $r^{1+}_{Na} = 139$ pm) and *B*-site ($r^{4+}_{Ti} = 60.5$ pm, $r^{5+}_{Nb} = 64$ pm).[34,35,55] Various theoretical models have been reported to explain the complex relaxor physics. Most of them suggest the presence of polar ordering in the form of PNR at short ranges exhibiting lower symmetry than that at long ranges.[32,41,56] The PNRs start to grow at T_B, and with the decrease in temperature, the intra-polar interactions (i.e., interaction among dipoles in a polar nano region) increase, leading to the increase in the size of PNRs.[41,57,58] On further lowering the temperature, PNRs start to freeze at a certain temperature referred to as freezing temperature, which is determined by using the Vogel–Fulcher relation,[59,60]

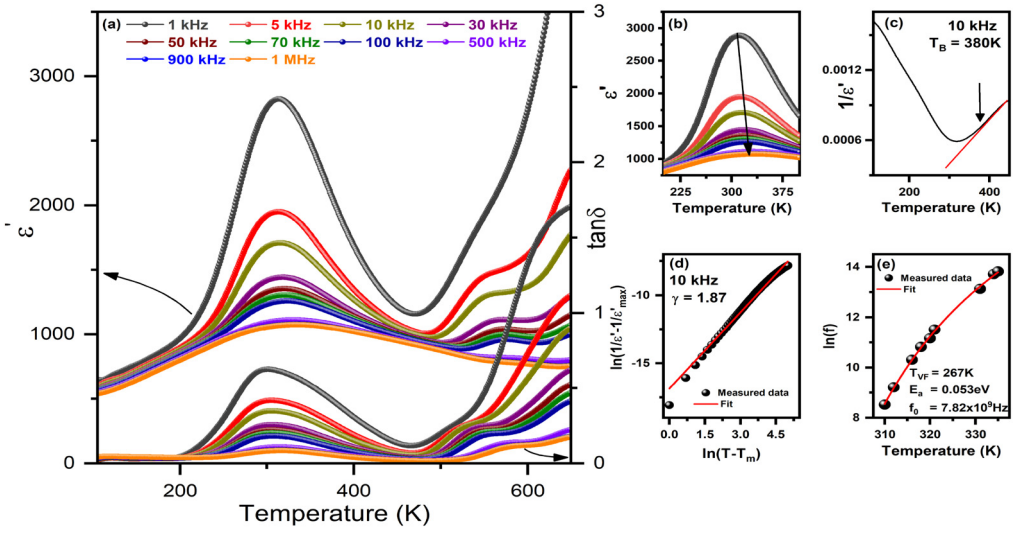

FIG. 2. (a) Temperature-dependent dielectric permittivity (ε') and loss ($\tan\delta$) plot at various frequencies, (b) the zoomed-up view of the observed frequency dispersion ($\Delta T \approx 27$ K) with the same order of frequency as in (a) and (c) Inverse of dielectric vs temperature plot at 10 kHz, (d) the linear fitting of $\ln(1/\varepsilon' - 1/\varepsilon'_{max})$ vs $\ln(T - T_m)$ at 10 kHz for KBST20 ceramic, and (e), the Vogel–Fulcher law fitting for KBST20 ceramic.

$$f = f_0 \exp[-E_a/k_B(T_m - T_{VF})], \quad (4)$$

where f and f_0 correspond to the measured frequency and pre-exponential factor, respectively, E_a is the activation energy, k_B is the Boltzmann constant, T_m is the temperature corresponding to dielectric maxima, and T_{VF} is the freezing temperature below which the dynamics of PNRs freeze. Figure 2(e) shows the Vogel–Fulcher fit and various parameters, viz., $T_{V\,F}$, E_a, and f_0 obtained for KBST20. The freezing of PNRs takes place below T_{VF} leading to inter-polar interactions (i.e., interactions among PNRs),[57] inferred from merging of temperature-dependent dielectric curves at different frequencies at low temperatures. This observation is supplemented by temperature-dependent hysteresis loops. The shape of the hysteresis loop at room temperature (Fig. 3) bears a resemblance to a linear lossy dielectric, indicating disorder within the system.[36] However, on lowering the temperature to 223 K (below $T_{V\,F}$) (Fig. 3), the shape of the loop is relaxor-like.[36] This change in the shape of the loop with temperature is suggestive of enhanced cationic (polar) ordering at low temperatures.

Now, an intuitive crystallographic model for KBST20 has been proposed to correlate ZTE with the increase in cationic ordering at low temperatures. At room temperature, the material is in a relatively disordered state where a significant amount of rattling space is available for smaller Ti^{4+} cations by the random distribution of surrounding Nb^{5+} cations, which are relatively larger in size.[26,27] In contrast, a much smaller rattling space is available at low temperatures due to cationic ordering.[26,27] Moreover, in the disordered state, the *B*-site cations rattle without distorting the neighboring oxygen octahedra. However, in an ordered state, the motion of *B*-site cations is constrained, which transfers octahedral stress to adjacent oxygen octahedra, leading to ferroelectrostriction.[26,27] Thus, we believe that the increase in correlations among ferroelectrostrictive PNRs results in zero thermal expansion at low temperatures. Furthermore, we have analyzed the temperature-dependent Raman data to comprehend the ZTE observed for KBST20 at low temperatures.

The presence of short-range atomic ordering in the long-range cubic phase is determined by temperature-dependent Raman spectroscopic analysis. Here, the host ceramic, viz., KNN50, is reported to possess a monoclinic structure with *Pm* space group at short ranges as well as long ranges with variations in lattice parameters/volume.[47,61–64] The room temperature Raman spectra for KBST20 shows Raman peaks similar to what has been reported earlier for KNN50, suggesting the presence of polar monoclinic distortions at short ranges for KBST20.[63,64] Figure 4(a) depicts the evolution of temperature-dependent Raman spectra for KBST20 ceramics with prominent peaks, viz., ≈ 245–265 cm^{-1} (ν_5), ≈ 525–553 cm^{-1} (ν_2), ≈ 585–610 cm^{-1} (ν_1), and ≈ 830–845 cm^{-1} ($\nu_1 + \nu_5$) present throughout. The peaks below 200 cm^{-1} correspond to translational modes of *A*-site cations similar to what has been observed for $NaNbO_3$ and $KNbO_3$.[65] The existence of polar distortions in BO_6 octahedra is clearly evident by the presence of ($\nu_1 + \nu_5$) peak in the Raman spectra.[66,67] This peak persists throughout the studied temperature range (77 K ≤ T ≤ 527 K) [Fig. 4(b)], confirming the presence of polar clusters up to the highest temperatures. Thus, the ferroelectrostrictive behavior observed for KBST20 having average cubic symmetry at long ranges has been attributed to the correlations among ferroelectrostrictive polar clusters (PNRs) (see the supplementary material for details). All the Raman peaks broaden with the increase in temperature, inferring thermal disorder in the system.[68,69] Figure 4(c) depicts the intensity variation of prominent Raman peaks as a function of temperature. The intensity of Raman peaks depends on various factors, viz., polarizability, presence of polar

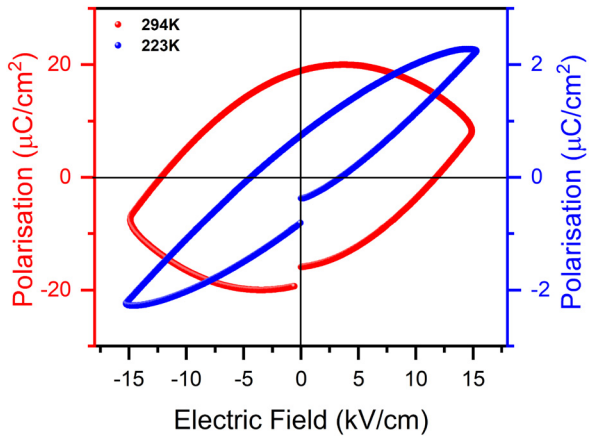

FIG. 3. Polarization vs electric field response of KBST20 ceramic at 294 and 223 K.

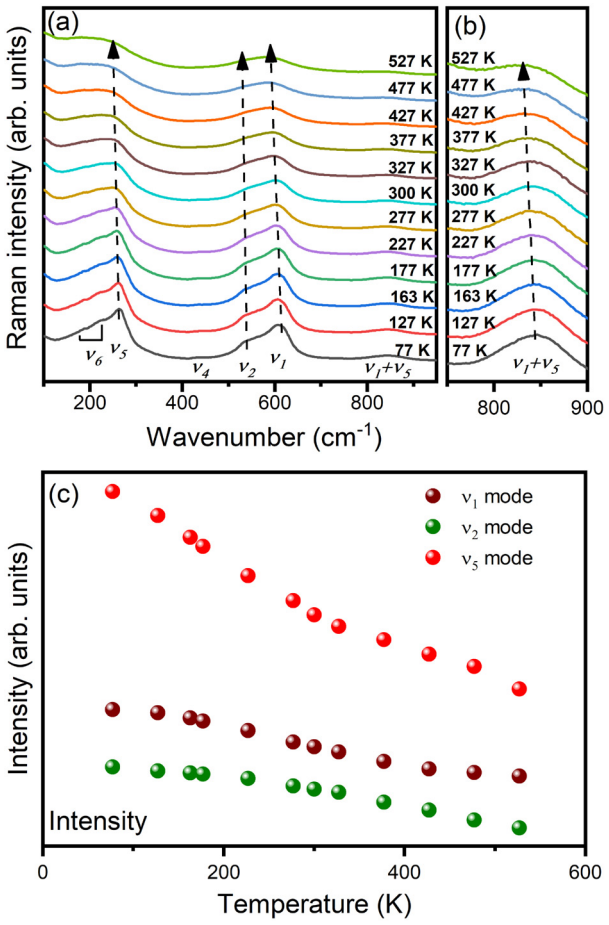

FIG. 4. (a) Temperature-dependent Raman data for KBST20 ceramic, (b) zoomed-up view of the polar peak ($\nu_1 + \nu_5$) as a function of temperature, and (c) the temperature-dependent intensity observed for prominent Raman modes (ν_1, ν_2, and ν_5).

phase, etc.[68,69] Here, we can see that the intensity of Raman modes increases [Fig. 4(c)] with the decrease in temperature, inferring the increase in polar phased regions at low temperatures, i.e., due to enhanced inter/intra polar interactions.[57] The enhanced short-range polar ordering with the increase in correlations (inter/intra polar cluster interactions) among PNRs at low temperatures are held responsible for ferroelectrostriction, consequently resulting in zero thermal expansion[57,58] in synthesized Pb-free smart material, viz., KBST20.

In conclusion, we have synthesized Pb-free relaxor ferroelectrics, i.e., KBST20 exhibiting zero thermal expansion (ZTE) for a wide temperature range ($T \leq 100$ K). The temperature-dependent volume of KBST20 deviates from linear behavior, i.e., PTE below the Burns temperature showing a significant volume gain at low temperatures, which has been attributed to the correlations among ferroelectrostrictive polar nano regions (PNRs). The ZTE has been quantified using the linear coefficient of thermal expansion (CTE), which is in the range of 0.255–5.75×10^{-6} K^{-1} (9–500 K). The relaxor properties of KBST20 have been analyzed using temperature-dependent dielectric data, demonstrating a relatively high relaxation ($\Delta T \approx 27$ K) compared to an earlier report on KBT20 ($\Delta T \approx 6$ K).[40] Owing to relaxor properties, the structures of KBST20 at long and short ranges were analyzed using temperature-dependent neutron diffraction and Raman scattering data, respectively. A centrosymmetric cubic structure was found to be stable at long ranges for $9\text{ K} \leq T \leq 500$ K. On the other hand, polar monoclinic distortions were confirmed at short ranges. Moreover, the enhancement in the polar phased regions (PNRs) at low temperatures is inferred by the integrated analysis of the datasets obtained using various techniques. We believe that the enhancement in the correlations among the PNRs with decreasing temperature leads to thermally induced ferroelectrostriction, consequently resulting in zero thermal expansion of KBST20.

See the supplementary material for the synthesis procedure, Le Bail fits, Debye–Grüneisen approximation, and deconvolution of temperature-dependent prominent Raman peaks.

S.T. acknowledges financial assistance from the Defence Research and Development Organisation (Grant No. ERIP/ER/202210003/M/01/1812) and DST-SERB, Government of India (Grant No. CRG/2021/006000). We acknowledge Mr. Gaurav Rudra Malik from the Department of Physics, Indian Institute of Technology (BHU) for technical assistance. The research was supported in part by the National Research Foundation of South Africa (Ref No. SRUG2205098188). A.P. acknowledges the financial support from the Friedel Sellschop fellowship of the University of the Witwatersrand, South Africa. J.A.A. thanks the Spanish Ministry for Science and Innovation (MCIN/AEI/10.13039/501100011033) for funding the Project PID2021-122477OB-I00. We are grateful to ILL for providing neutron beam time and to SPINs (Universidad of Zaragoza, Spain) for financial support for the neutron experiment.

AUTHOR DECLARATIONS

Conflict of Interest

The authors have no conflicts to disclose.

Author Contributions

Anuvrat Tripathi: Conceptualization (supporting); Data curation (lead); Formal analysis (equal); Investigation (equal); Methodology (equal); Software (equal); Validation (equal); Visualization (equal); Writing – original draft (lead); Writing – review & editing (supporting). **Abhishek Pandey:** Formal analysis (supporting); Writing – original draft (supporting); Writing – review & editing (supporting). **Jose Antonio Alonso:** Data curation (supporting); Writing – review & editing (supporting). **Rudolph Erasmus:** Data curation (supporting); Writing – review & editing (supporting). **Maria Teresa Fernández-Díaz:** Data curation (supporting). **Saurabh Tripathi:** Conceptualization (lead); Data curation (supporting); Formal analysis (equal); Funding acquisition (lead); Investigation (equal); Methodology (equal); Project administration (lead); Resources (lead); Software (equal); Supervision (lead); Validation (equal); Visualization (equal); Writing – original draft (supporting); Writing – review & editing (lead).

DATA AVAILABILITY

The data that support the findings of this study are available within the article and its supplementary material.

REFERENCES

[1]S. Tawfick, M. De Volder, D. Copic, S. J. Park, C. R. Oliver, E. S. Polsen, M. J. Roberts, and A. J. Hart, Adv. Mater. **24**, 1628 (2012).
[2]A. Atkinson, S. Barnett, R. J. Gorte, J. Irvine, A. J. McEvoy, M. Mogensen, S. C. Singhal, and J. Vohs, Nat. Mater. **3**, 17 (2004).
[3]G. H. Haertling, J. Am. Ceram. Soc. **82**, 797 (1999).
[4]V. Ravi, S. Firdosy, T. Caillat, E. Brandon, K. Van Der Walde, L. Maricic, and A. Sayir, J. Electron. Mater. **38**, 1433 (2009).
[5]C. Hunter, Surf. Mount Technol. **18**, 16 (2004).
[6]J.-P. Locquet, J. Perret, J. Fompeyrine, E. Mächler, J. W. Seo, and G. Van Tendeloo, Nature **394**, 453 (1998).
[7]T. A. Mary, J. Evans, T. Vogt, and A. Sleight, Science **272**, 90 (1996).
[8]B. K. Greve, K. L. Martin, P. L. Lee, P. J. Chupas, K. W. Chapman, and A. P. Wilkinson, J. Am. Chem. Soc. **132**, 15496 (2010).
[9]M. van Schilfgaarde, I. Abrikosov, and B. Johansson, Nature **400**, 46 (1999).
[10]Y. Song, Y. Qiao, Q. Huang, C. Wang, X. Liu, Q. Li, J. Chen, and X. Xing, Chem. Mater. **30**, 6236 (2018).
[11]N. Anshukova, B. Bulychev, A. Golovashkin, L. Ivanova, I. Krynetskii, A. Minakov, and A. Rusakov, J. Exp. Theor. Phys. **97**, 70 (2003).
[12]H. Fujishita, Y. Hayashi, M. Saito, H. Unno, H. Kaneko, H. Okamoto, M. Ohashi, Y. Kobayashi, and M. Sato, Eur. Phys. J. B **85**, 1 (2012).
[13]X. Xing, J. Deng, J. Chen, and G. Liu, Rare Metals **22**, 294 (2003).
[14]J. Chen, X. Xing, R. Yu, and G. Liu, J. Am. Ceram. Soc. **88**, 1356 (2005).
[15]Z. Pan, J. Chen, X. Jiang, L. Hu, R. Yu, H. Yamamoto, T. Ogata, Y. Hattori, F. Guo, X. Fan *et al.*, J. Am. Chem. Soc. **139**, 14865 (2017).
[16]J. Forrester, E. Kisi, K. Knight, and C. Howard, J. Phys.: Condens. Matter **18**, L233 (2006).
[17]S. P. Singh, D. Pandey, S. Yoon, S. Baik, and N. Shin, Appl. Phys. Lett. **90**, 182910 (2007).
[18]T. Maiti, R. Guo, and A. Bhalla, J. Am. Ceram. Soc. **91**, 1769 (2008).
[19]P. Bonneau, P. Garnier, G. Calvarin, E. Husson, J. Gavarri, A. Hewat, and A. Morell, J. Solid State Chem. **91**, 350 (1991).
[20]J. Zhao, A. Glazounov, Q. Zhang, and B. Toby, Appl. Phys. Lett. **72**, 1048 (1998).
[21]J. Chen, L. Hu, J. Deng, and X. Xing, Chem. Soc. Rev. **44**, 3522 (2015).
[22]Y. Kuroiwa, S. Aoyagi, A. Sawada, J. Harada, E. Nishibori, M. Takata, and M. Sakata, Phys. Rev. Lett. **87**, 217601 (2001).
[23]T. Yang, Y. Wang, L. Fan, N. Wang, K. Lin, J. Chen, and X. Xing, J. Phys. Chem. C **124**, 20445 (2020).
[24]G. Shirane and A. Takeda, J. Phys. Soc. Jpn. **7**, 1 (1952).
[25]S. Kawamura, E. Magome, C. Moriyoshi, Y. Kuroiwa, N. Taniguchi, H. Tanaka, and S. Wada, Ferroelectrics **462**, 1 (2014).
[26]K. Uchino, L. Cross, R. Newnham, and S. Nomura, Phase Transitions **1**, 333 (1980).

[27]K. Uchino, S. Nomura, L. E. Cross, R. E. Newnham, and S. J. Jang, J. Mater. Sci. **16**, 569 (1981).
[28]F. Sayetat, P. Fertey, and M. Kessler, J. Appl. Crystallogr. **31**, 121 (1998).
[29]F. Reif, *Fundamentals of Statistical and Thermal Physics* (Waveland Press, 2009).
[30]L. K. Pradhan and M. Kar, *Multifunctional Ferroelectric Materials*, edited by D. R. Sahu (IntechOpen, Rijeka, 2021), Chap. 4.
[31]A. Bhalla, R. Guo, and R. Roy, Mater. Res. Innovations **4**, 3 (2000).
[32]L. E. Cross, Ferroelectrics **76**, 241 (1987).
[33]C. W. Ahn, C.-H. Hong, B.-Y. Choi, H.-P. Kim, H.-S. Han, Y. Hwang, W. Jo, K. Wang, J.-F. Li, J.-S. Lee *et al.*, J. Korean Phys. Soc. **68**, 1481 (2016).
[34]A. A. Bokov and Z.-G. Ye, J. Adv. Dielectr. **2**, 1241010 (2012).
[35]D. Alikin, A. Turygin, A. Kholkin, and V. Shur, Materials **10**, 47 (2017).
[36]D. B. Migas, V. A. Turchenko, A. Rutkauskas, S. V. Trukhanov, T. I. Zubar, D. I. Tishkevich, A. V. Trukhanov, and N. V. Skorodumova, J. Mater. Chem. C **11**, 12406 (2023).
[37]P. Gehring, S. Wakimoto, Z.-G. Ye, and G. Shirane, Phys. Rev. Lett. **87**, 277601 (2001).
[38]S. Choi, R. T. Shrout, S. Jang, and A. Bhalla, Ferroelectrics **100**, 29 (1989).
[39]Z. Yu, C. Ang, R. Guo, and A. Bhalla, J. Appl. Phys. **92**, 2655 (2002).
[40]Y. Yang, Y. Ji, M. Fang, Z. Zhou, L. Zhang, and X. Ren, Phys. Rev. Lett. **123**, 137601 (2019).
[41]H. Du, W. Zhou, F. Luo, D. Zhu, S. Qu, and Z. Pei, J. Appl. Phys. **105**, 124104 (2009).
[42]S. Sahoo, D. K. Pradhan, S. Kumari, K. S. Samantaray, C. Singh, A. Mishra, M. M. Rahaman, B. Behera, A. Kumar, R. Thomas *et al.*, Sci. Rep. **13**, 19096 (2023).
[43]A. Bokov and Z.-G. Ye, J. Mater. Sci. **41**, 31 (2006).
[44]T. Rojac, Commun. Mater. **4**, 12 (2023).
[45]A. K. Singh, D. N. Dubey, G. Singh, and S. Tripathi, Appl. Phys. Lett. **116**, 232902 (2020).
[46]L. Egerton and D. M. Dillon, J. Am. Ceram. Soc. **42**, 438 (1959).
[47]J. Kong, J. Liu, F. Marlton, M. Jørgensen, and A. Pramanick, Phys. Rev. B **103**, 184104 (2021).
[48]M. Kumar, A. Garg, R. Kumar, and M. Bhatnagar, Physica B **403**, 1819 (2008).
[49]A. Ianculescu, I. Pintilie, C. Vasilescu, M. Botea, A. Iuga, A. Melinescu, N. Drăgan, and L. Pintilie, Ceram. Int. **42**, 10338 (2016).
[50]W. Li, Z. Xu, R. Chu, P. Fu, and J. Hao, J. Alloys Compd. **499**, 255 (2010).
[51]S. Gel, J. Mater. Environ. Sci **8**, 4945 (2017).
[52]J. Rodríguez-Carvajal, Physica B **192**, 55 (1993).
[53]J. Chen, F. Wang, Q. Huang, L. Hu, X. Song, J. Deng, R. Yu, and X. Xing, Sci. Rep. **3**, 2458 (2013).
[54]K. Uchino, in *Advanced Piezoelectric Materials* (Elsevier, 2017) pp. 127–153.
[55]R. D. Shannon, Acta Crystallogr., Sect. A **32**, 751 (1976).
[56]I. Chen, J. Phys. Chem. Solids **61**, 197 (2000).
[57]D. N. Dubey, G. Singh, and S. Tripathi, J. Phys. D: Appl. Phys. **54**, 365304 (2021).
[58]H. Kumar and S. Tripathi, J. Phys. D: Appl. Phys. **57**(33), 335502 (2024).
[59]D. Viehland, S. Jang, L. E. Cross, and M. Wuttig, J. Appl. Phys. **68**, 2916 (1990).
[60]X. Long and Z.-G. Ye, Appl. Phys. Lett. **90**, 112905 (2007).
[61]S. Gupta, V. Petkov, and S. Priya, Appl. Phys. Lett. **105**, 232902 (2014).
[62]Z. Wang, H. Gu, Y. Hu, K. Yang, M. Hu, D. Zhou, and J. Guan, CrystEngComm **12**, 3157 (2010).
[63]S. Kojima, J. Zushi, Y. Noguchi, and M. Miyayama, Ferroelectrics **532**, 183 (2018).
[64]M. Asif Rafiq, P. Supancic, M. Elisabete Costa, P. M. Vilarinho, and M. Deluca, Appl. Phys. Lett. **104**, 011902 (2014).
[65]R. Singh, K. Kambale, A. R. Kulkarni, and C. Harendranath, Mater. Chem. Phys. **138**, 905 (2013).
[66]L. Veselinović, M. Mitrić, L. Mančić, M. Vukomanović, B. Hadžić, S. Marković, and D. Uskoković, J. Appl. Crystallogr. **47**, 999 (2014).
[67]I. Margaritescu, K. Datta, J. Chen, and B. Mihailova, J. Raman Spectrosc. **51**, 1200 (2020).
[68]M. Deluca, H. Hu, M. N. Popov, J. Spitaler, and T. Dieing, Commun. Mater. **4**, 78 (2023).
[69]H. Yu, L. Chen, C. Zhou, and H. Qi, Crystals **13**, 751 (2023).